ELECTRON BEAM LOSS IN COMMERCIAL ESEM

Gerasimos D Danilatos[1], Matthew R Phillips[2], John V Nailon[3]

[1]ESEM Research Laboratory, 98 Brighton Boulevard, North Bondi, NSW 2026, AUSTRALIA
[2]Microstructural Analysis Unit, University of Technology, Sydney, PO Box 123, Broadway, NSW 2007, AUSTRALIA
[3]Centre for Microscopy and Microanalysis, The University of Queensland, Brisbane, Qld 4072, AUSTRALIA

Abstract

Introduction

Conventional differential pumping is used on present day commercial environmental scanning electron microscope (ESEM) instruments to separate the high vacuum of the electron optics column from the high pressure specimen chamber. A transition region of intermediate pressures is established between the two extreme regions of the microscope. The electron beam is transferred from the high vacuum to the high pressure via a transition region in which the beam undergoes collisions with the gas and suffers initial electron losses. The loss of electrons in the transition region is an inevitable consequence of the differential pumping method used. In particular, the magnitude of electron loss is determined by the design of a given instrument and can be greater or equal to some physical limit imposed by the formation of a supersonic gas jet downstream of the pressure-limiting aperture (PLA).

An early experimental prototype of ESEM was designed and operated at the physical limit of minimum electron beam loss in the transition region (Danilatos 1981). The optimum condition was determined by experiment to be the case when (a) the wall thickness of the PLA was much less than its diameter and (b) the conductance of the downstream evacuation pipe was as large as possible to allow minimum back-pressure downstream of the transition region. The relatively thin walled PLA was obtained by the use of commercially available copper grid apertures of different diameters. The reported thickness of PLA wall was 10 μm and 30 μm. A detailed experimental study of the behaviour of such apertures including the formation of a supersonic jet was later reported by Danilatos (1983), while all subsequent work by the present author has applied the same principles (Danilatos, 1993).

The consequence of correctly applying differential pumping together with appropriate detection techniques has allowed ESEM to operate at any pressure between vacuum and one atmosphere. Different applications require different specimen chamber pressures, which can be divided in various utilitarian (functional, or practical) pressure ranges, such as: (a) Pressure sufficient to suppress charging effects, usually up to around 200 Pa; (b) pressure sufficient to maintain liquid water phase, i.e. greater than 609 Pa; (c) pressure corresponding to the saturation water vapor pressure at room temperature, i.e. around 2 kPa; (d) saturation water vapor pressure at "body" temperature, i.e. around 6 kPa; (e) gas pressure that allows animal life, i.e. around 20-100 kPa.

Two commercial ESEM instruments have been evaluated in regard to gas density variation and electron beam loss in the transition region of their differential pumping systems, and a comparison is made to the prototype ESEM operating at the optimum condition. This study has been prompted by concerns that a significant deviation from expected standards has been found in practice. This deviation consists in lower signal-to-noise-ratio at a given pressure and in lower upper pressure limit of operation at a given accelerating voltage, for each instrument. It is shown that an unnecessary deterioration of performance is due, by and large, to a departure from the optimum geometry design of the apertures.

Materials and Methods

In order to find the properties of the gas flow through a PLA, an alternative to the experimental techniques employed in past work is to theoretically calculate them. However, the calculation was not always possible or practical, because analytical formulations of the gas flow exist only for the extreme cases of either continuum flow (high pressures/small apertures) or free molecular flow (low pressure/large apertures). The conditions of ESEM operation correspond to the transition region between continuum and free molecular flow. Even where analytical solutions are applicable, the optimum ESEM geometry corresponds to very difficult or impractical cases to solve analytically. Fortunately, the gas flow properties can be computed by simulation techniques such as the direct simulation by Monte Carlo (DSMC) method developed by Bird (1985).

The DSMC method is a technique for the computer modelling of a real gas by some thousands, or even millions of simulated molecules depending on the gas pressure and the physical extent of the flow field. The velocities and positions of these molecules are stored in the computer and are modified with time as the molecules move and collide through the boundaries defining the flow field. The initial entry and exit conditions for a given gas are set and the program computes the gas properties until it reaches a steady state situation, whereupon the program continues to sample the equilibrium properties until a satisfactory smooth average for each field point is achieved. These programs were initially developed for space engineering problems involving large space vehicles in

rarefied gas conditions, and required the use of mainframe computers. The availability of fast and cheap personal computers, which can be devoted to solve DSMC problems, has allowed this technique to be adapted and used by the present author for gas flow computations in the ESEM (Danilatos 1991, 1993). The same technique is used in the present work to compute three cases of PLA configurations and the associated gas density variation.

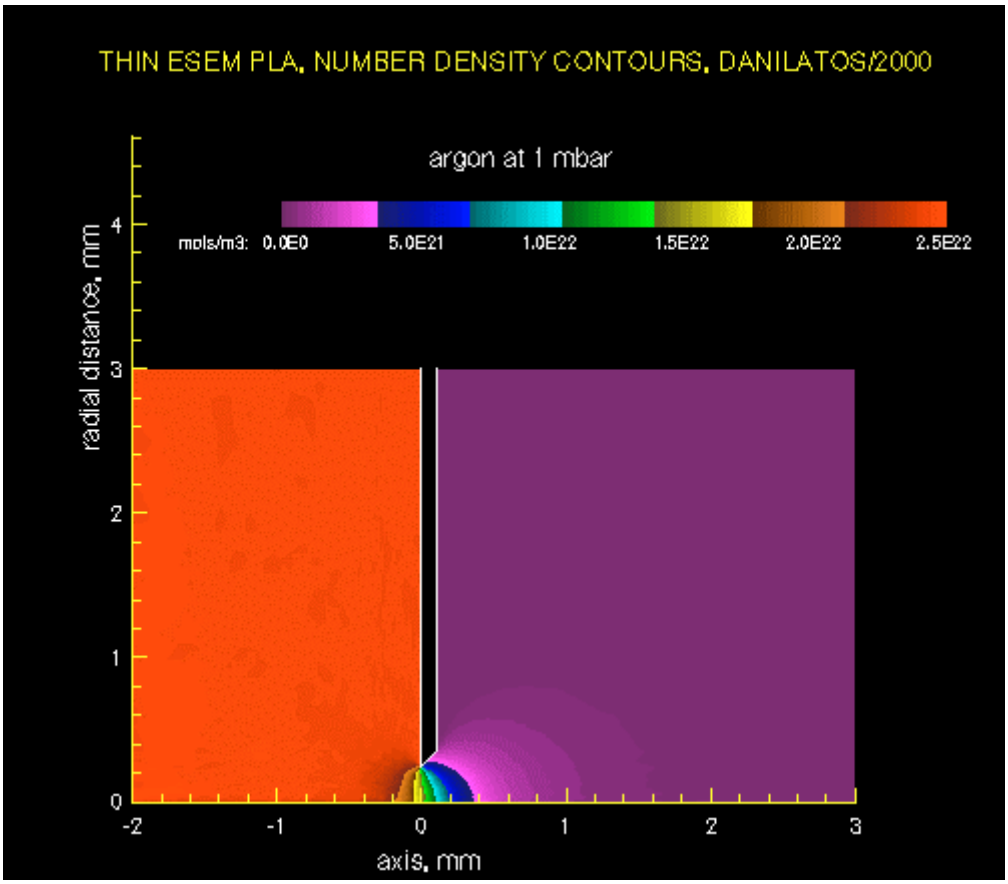

Fig. 1 Semi-cross-section of thin plate PLA with density contours of argon flowing from left (with specimen chamber pressure at 1mbar=100 Pa) to right (with pump at 0.00 Pa).

The first case involves a 0.5 mm diameter PLA on a 0.1 mm thick plate with the rim of the aperture tapered at 45 degrees angle, which diverges in the downstream direction of the gas flow. This geometry of PLA together with the gas flow is shown in Fig. 1, where only half of the PLA cross-section is drawn on one side of the aperture axis, because the flow field is axially symmetric. The specimen chamber of the ESEM is located on the left-hand side and the leaking gas through the aperture is pumped out from the right had side. The electron beam travels along the axis.

The second case involves the PLA assembly of an ElectroScan U3 model ESEM employed by the University of Queensland (QLD) since 1991, the axisymmetrical semi-cross-section of which is drawn in Fig. 2. Similarly, the specimen chamber is located on the left-hand side of the drawing whereby gas enters from side CR and exits from side IJ. Some gas also exits from the second PLA formed on plate LM. The electron beam travels along the axis RQ.

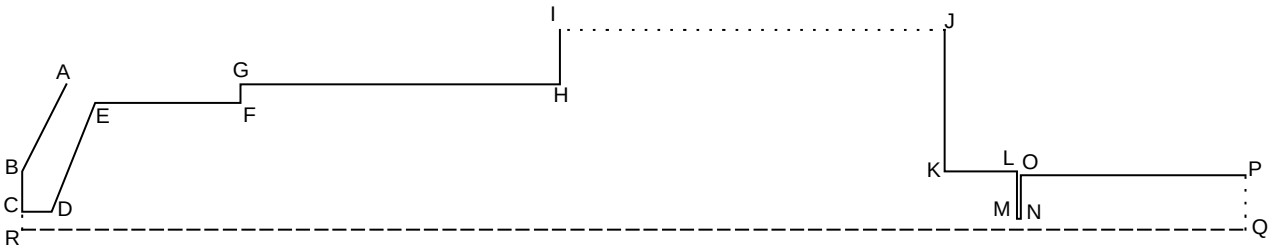

Fig. 2 Drawing of the geometry of the internal "bullet" assembly for the QLD) ESEM. Line RQ is an axis of symmetry. The point coordinates are A(0.6, 2.0), B(0.0, 0.8), C(0.0, 0.25), D(0.4, 0.25), E(1.0, 1.75), F(3.0, 1.75), G(3.0, 2.0), H(7.4, 2.0), I(7.4, 2.75), J(12.7, 2.75), K(12.7, 0.8), L(13.7, 0.8), M(13.7, 0.15), N(13.75, 0.15), O(13.75, 0.75), P(16.85, 0.75), Q(16.85, 0.0), R(0.0, 0.0).

The third case involves the PLA assembly of a Philips XL30 ESEM employed by the University of Technology, Sydney (UTS), since 1999, the axisymmetrical cross-section of which is drawn in Fig. 3. Similarly, the specimen chamber is located on the left-hand side of the drawing whereby gas enters from side CU and exits from side LM. Some gas also exits from the second PLA formed on plate OP. The electron beam travels along the axis UT.

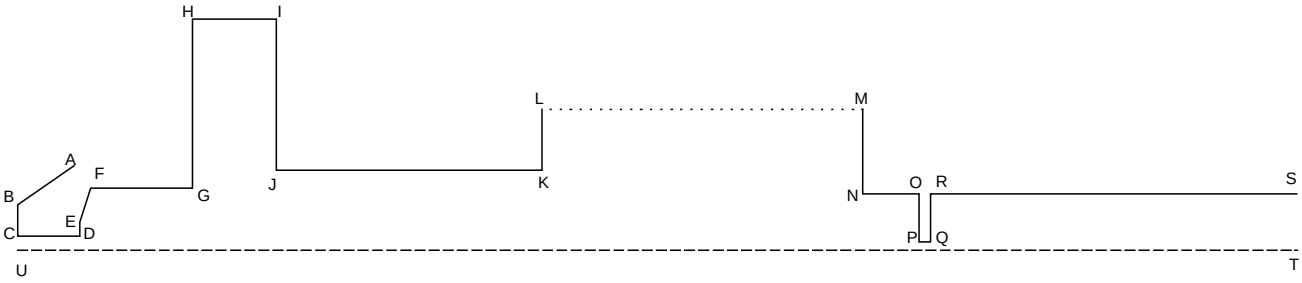

Fig. 3. Drawing of the internal geometry of the "bullet" assembly of the ESEM at UTS. Line UT is the axis of symmetry. The point coordinates are A(1.0, 1.5), B(0.0, 0.8), C(0.0, 0.25), D(1.1, 0.25), E(1.1, 0.5), F(1.3, 1.1), G(3.1, 1.1), H(3.1, 4.1), I(4.6, 4.1), J(4.6, 1.42), K(9.3, 1.42), L(9.3, 2.5), M(15.0, 2.5), N(15.0, 1.0), O(16.0, 1.0), P(16.0, 0.15), Q(16.2, 0.15), R(16.2, 1.0), S(22.7, 1.0), T(22.7, 0.0), U(0.0, 0.0).

The electron beam encounters gas molecules with which it collides well before it enters in the specimen chamber. A gas plume or jet forms downstream (or "above") of the PLA plane. The gas density decreases rapidly along the axis of the jet but the precise variation of density depends on the geometry of walls within which the gas is constrained. The fastest density decrease is expected to occur in the first case (Fig. 1) but a quantitative evaluation of this phenomenon is necessary in order to establish the actual consequences on imaging. The latter is achieved by finding the amount of electron scattering in the plume by the use of electron scattering collision theory.

The electron beam scattering process is governed by the Poisson distribution probability $P(x)$

$$P(x) = \frac{m^x e^{-m}}{x!}$$

which gives the probability for an electron to undergo x number of collisions, when the average number of collisions per electron is m. Knowledge of the parameter m allows us to immediately find the electron beam current I that is transmitted completely without any scattering by the gas molecules, when the initial incident beam current in vacuum is I_0. The fraction of transmitted beam is given by the exponential equation

$$\frac{I}{I_0} = e^{-m}$$

The parameter m is found from the function of number density $n(z)$ along the axis z and the total scattering cross-section σ_T of the gas:

$$m = \sigma_T \int n(z) dz$$

The integration above is performed between any two limits defining the gas layer of interest. In the present situation, we integrate from the entrance interface of the PLA up to a point where the density is essentially reduced to a negligible value. As upper limit of integration we take 10 mm for the first case corresponding to Fig. 1 (thin PLA), 13.7 mm for the second case (QLD) and 16 mm for the third case (UTS). In the latter two cases we use the location of the second PLA shown in Figs. 2 and 3 as the upper limit of integration. The integral factor can be referred to as the molecular thickness (mol_thick) corresponding to the customary term of mass thickness (i.e. density times thickness) in other microscopy works, namely:

$$mol\_thick = \int n(z)dz$$

The mathematical analysis presented is absolutely correct, but, in practice, the predicted values are reliable to the extent that the supplied values of total scattering cross-section and density variation are correct. The DSMC method has been shown to be very reliable in practice so that the supplied value of the total scattering cross-section alone determines the accuracy of the electron beam loss provided in this work. Argon is used as the test gas, because its scattering cross-section can be derived analytically as a monatomic gas (see, for example Jost and Kessler, 1963; Danilatos, 1988) and the values used are tabulated for different accelerating voltages below. However, one of the main aims of this work is to produce the gas density variation, from which the molecular thickness is found. The latter can be used alone to evaluate instrument performance from the total amount of gas in the electron beam path "above" the PLA.

The specimen chamber and the pressure at the exit boundaries of the system are set to a desired value and the computer finds the density at each point inside the flow field. Because there is a depletion zone immediately upstream (i.e. "below") of the PLA plane, the entry gas boundary is set 2 mm further upstream, where the density is essentially equal to the stagnation density in the specimen chamber held at 293 K temperature. Along with the density, the computer also finds the temperature, velocity and Mach number at every point of the field, and leak rate of gas through various interfaces, such as through the PLA. These and other characteristics will be included in a more comprehensive report to be released in due course, later.

Results

Two specimen chamber pressures are considered, namely, 100 Pa and 1000 Pa, which are typical of commercial ESEM operation at present. As far as the first case of Fig. 1 is concerned, the back-pressure at the pump is set to 0 Pa which corresponds to an ideal limiting case. We consider four accelerating voltages and the results are given in Table 1.

THIN PLA						
p , Pa	p_1, Pa	mol_thick mols/m²	E , eV	σ_T , m²	m	$\frac{I}{I_0}$
100	0	4.00E+18	5000	1.56E-20	0.06255	0.939
100	0	4.00E+18	10000	8.28E-21	0.03316	0.967
100	0	4.00E+18	15000	5.73E-21	0.02295	0.977
100	0	4.00E+18	20000	4.43E-21	0.01774	0.982
1000	0	5.69E+19	5000	1.56E-20	0.88874	0.411
1000	0	5.69E+19	10000	8.28E-21	0.47111	0.624
1000	0	5.69E+19	15000	5.73E-21	0.32602	0.722
1000	0	5.69E+19	20000	4.43E-21	0.25206	0.777

Table 1 Corresponding values of specimen chamber pressure p, pump pressure p_1, molecular thickness mol_thick, accelerating voltage E, total scattering cross-section σ_T, average number of collisions m, transmitted fraction of beam $\frac{I}{I_0}$ for a thin PLA.

The back-pressure at the exit interfaces is not exactly known for the given instruments but four typical values are chosen for the interface where the differential pump acts (below, referred to as pump pressure). These four pump pressures are expected to cover a range within which the real situation falls. These values are 0, 1, 2 and 4 Pa when the specimen chamber pressure is 100 Pa, and 0, 10, 20 and 40 Pa when the specimen chamber pressure is 1000 Pa. The pressure at the second PLA interface with the rest of the electron optics column is assumed to be zero in all cases. Therefore, there are eight combinations of pressure for each commercial instrument, which are given in Table 2 for the QLD instrument and in Table 3 for the UTS instrument, also at four accelerating voltages.

UNIVERSITY OF QUEENSLAND ESEM (U3)						
p , Pa	p_1, Pa	mol_thick mols/m^2	E , eV	σ_T , m^2	m	$\frac{I}{I_0}$
100	0	9.70E+18	5000	1.56E-20	0.15144	0.859
100	0	9.70E+18	10000	8.28E-21	0.08028	0.923
100	0	9.70E+18	15000	5.73E-21	0.05555	0.946
100	0	9.70E+18	20000	4.43E-21	0.04295	0.958
100	1	1.31E+19	5000	1.56E-20	0.20479	0.815
100	1	1.31E+19	10000	8.28E-21	0.10856	0.897
100	1	1.31E+19	15000	5.73E-21	0.07512	0.928
100	1	1.31E+19	20000	4.43E-21	0.05808	0.944
100	2	1.61E+19	5000	1.56E-20	0.25125	0.778
100	2	1.61E+19	10000	8.28E-21	0.13318	0.875
100	2	1.61E+19	15000	5.73E-21	0.09217	0.912
100	2	1.61E+19	20000	4.43E-21	0.07126	0.931
100	4	2.23E+19	5000	1.56E-20	0.34792	0.706
100	4	2.23E+19	10000	8.28E-21	0.18443	0.832
100	4	2.23E+19	15000	5.73E-21	0.12763	0.880
100	4	2.23E+19	20000	4.43E-21	0.09867	0.906
1000	0	1.28E+20	5000	1.56E-20	1.99329	0.136
1000	0	1.28E+20	10000	8.28E-21	1.05662	0.348
1000	0	1.28E+20	15000	5.73E-21	0.73121	0.481
1000	0	1.28E+20	20000	4.43E-21	0.56532	0.568
1000	10	1.50E+20	5000	1.56E-20	2.33592	0.097
1000	10	1.50E+20	10000	8.28E-21	1.23824	0.290
1000	10	1.50E+20	15000	5.73E-21	0.85690	0.424
1000	10	1.50E+20	20000	4.43E-21	0.66249	0.516
1000	20	1.75E+20	5000	1.56E-20	2.73466	0.065
1000	20	1.75E+20	10000	8.28E-21	1.44962	0.235
1000	20	1.75E+20	15000	5.73E-21	1.00318	0.367
1000	20	1.75E+20	20000	4.43E-21	0.77558	0.460
1000	40	2.34E+20	5000	1.56E-20	3.65359	0.026
1000	40	2.34E+20	10000	8.28E-21	1.93673	0.144
1000	40	2.34E+20	15000	5.73E-21	1.34027	0.262
1000	40	2.34E+20	20000	4.43E-21	1.03620	0.355

Table 2 Corresponding values of specimen chamber pressure p, pump pressure p_1, molecular thickness mol_thick, accelerating voltage E, total scattering cross-section σ_T, average number of collisions m, transmitted fraction of beam $\frac{I}{I_0}$ for the University of Queensland ESEM.

UNIVERSITY OF TECHNOLOGY, SYDNEY, ESEM (PHILIPS XL30)						
p , Pa	p_1, Pa	mol_thick mols/m^2	E , eV	σ_T , m^2	m	$\frac{I}{I_0}$
100	0	2.105E+19	5000	1.56E-20	0.32875	0.720
100	0	2.105E+19	10000	8.28E-21	0.17427	0.840
100	0	2.105E+19	15000	5.73E-21	0.12060	0.886
100	0	2.105E+19	20000	4.43E-21	0.09324	0.911
100	1	2.336E+19	5000	1.56E-20	0.36496	0.694
100	1	2.336E+19	10000	8.28E-21	0.19346	0.824
100	1	2.336E+19	15000	5.73E-21	0.13388	0.875
100	1	2.336E+19	20000	4.43E-21	0.10351	0.902
100	2	2.705E+19	5000	1.56E-20	0.42249	0.655
100	2	2.705E+19	10000	8.28E-21	0.22396	0.799
100	2	2.705E+19	15000	5.73E-21	0.15498	0.856
100	2	2.705E+19	20000	4.43E-21	0.11982	0.887
100	4	3.318E+19	5000	1.56E-20	0.51824	0.596
100	4	3.318E+19	10000	8.28E-21	0.27471	0.760
100	4	3.318E+19	15000	5.73E-21	0.19011	0.827
100	4	3.318E+19	20000	4.43E-21	0.14698	0.863
1000	0	2.691E+20	5000	1.56E-20	4.20410	0.015
1000	0	2.691E+20	10000	8.28E-21	2.22855	0.108
1000	0	2.691E+20	15000	5.73E-21	1.54222	0.214
1000	0	2.691E+20	20000	4.43E-21	1.19233	0.304
1000	10	2.888E+20	5000	1.56E-20	4.51102	0.011
1000	10	2.888E+20	10000	8.28E-21	2.39124	0.092
1000	10	2.888E+20	15000	5.73E-21	1.65481	0.191
1000	10	2.888E+20	20000	4.43E-21	1.27937	0.278
1000	20	3.113E+20	5000	1.56E-20	4.86233	0.008
1000	20	3.113E+20	10000	8.28E-21	2.57747	0.076
1000	20	3.113E+20	15000	5.73E-21	1.78368	0.168
1000	20	3.113E+20	20000	4.43E-21	1.37901	0.252
1000	40	3.724E+20	5000	1.56E-20	5.81746	0.003
1000	40	3.724E+20	10000	8.28E-21	3.08378	0.046
1000	40	3.724E+20	15000	5.73E-21	2.13406	0.118
1000	40	3.724E+20	20000	4.43E-21	1.64990	0.192

Table 3 Corresponding values of specimen chamber pressure p, pump pressure p_1, molecular thickness mol_thick, accelerating voltage E, total scattering cross-section σ_T, average number of collisions m, transmitted fraction of beam $\frac{I}{I_0}$ for the University of Technology, Sydney, ESEM.

Graphical representations of some typical cases are also given below. Fig. 4 shows the variation of gas particle density (atoms per cubic meter) along the axis of the three systems, when the specimen chamber is held at 100 Pa and the

pump pressure is 0 Pa. Each curve represents the average density of four radial positions along the axis, namely, at 0.05, 0.10, 0.15 and 0.20 mm, where the density varies slightly.

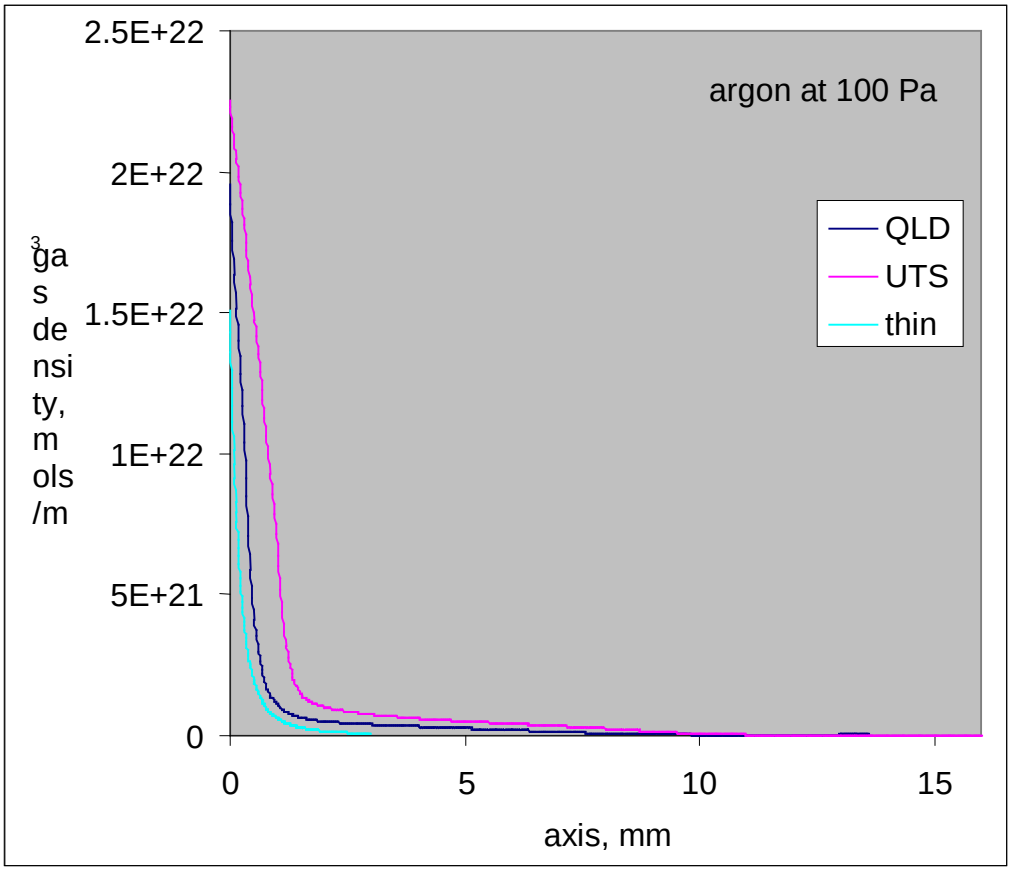

Fig. 4 Density variation of the jet of argon downstream of the PLA plane along the axis for the "thin", QLD and UTS systems, starting at 100 Pa in the upstream specimen chamber.

Fig. 5 shows the density variation along the jet axis for the three systems when the specimen chamber pressure is 1000 Pa and the pump pressure is 0 Pa.

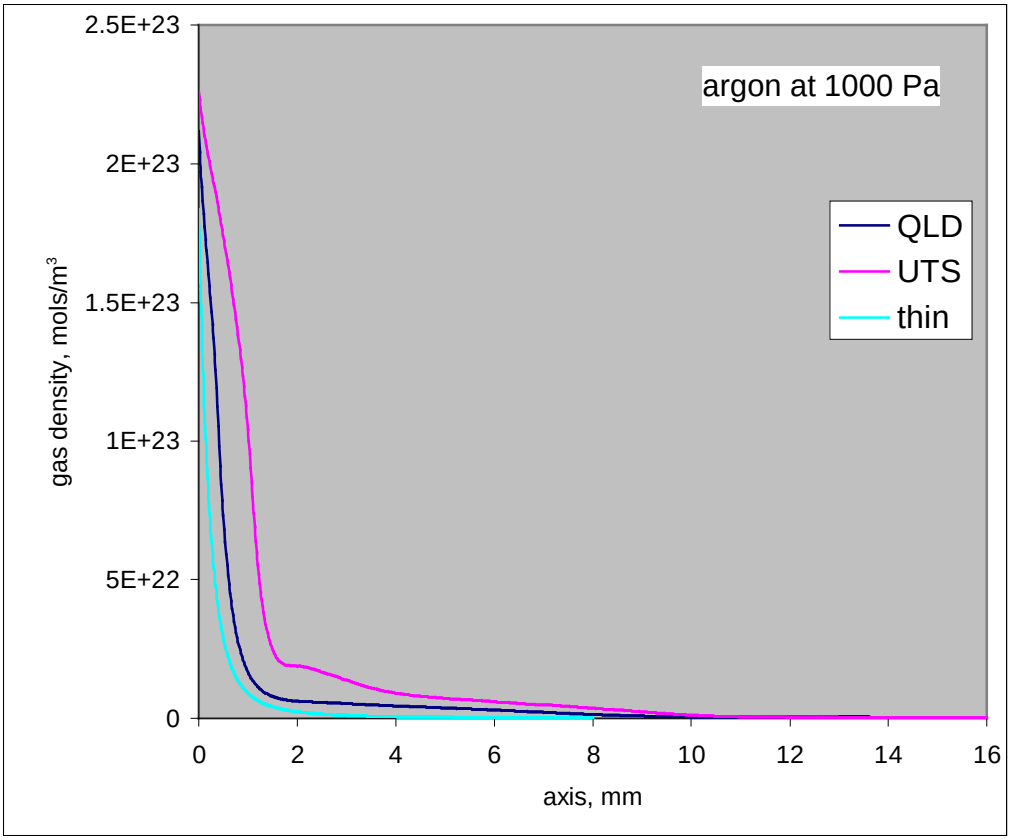

Fig. 5 Density variation of the jet of argon downstream of the PLA plane along the axis for the "thin", QLD and UTS systems, starting at 1000 Pa in the upstream specimen chamber.

Fig 6 shows the variation of gas density along the axis of the QLD system, when the specimen chamber is held at 100 Pa and the pump pressure is 0, 1, 2 and 4 Pa. For comparison, the ideal case curve (at 0 Pa pump pressure) is also included.

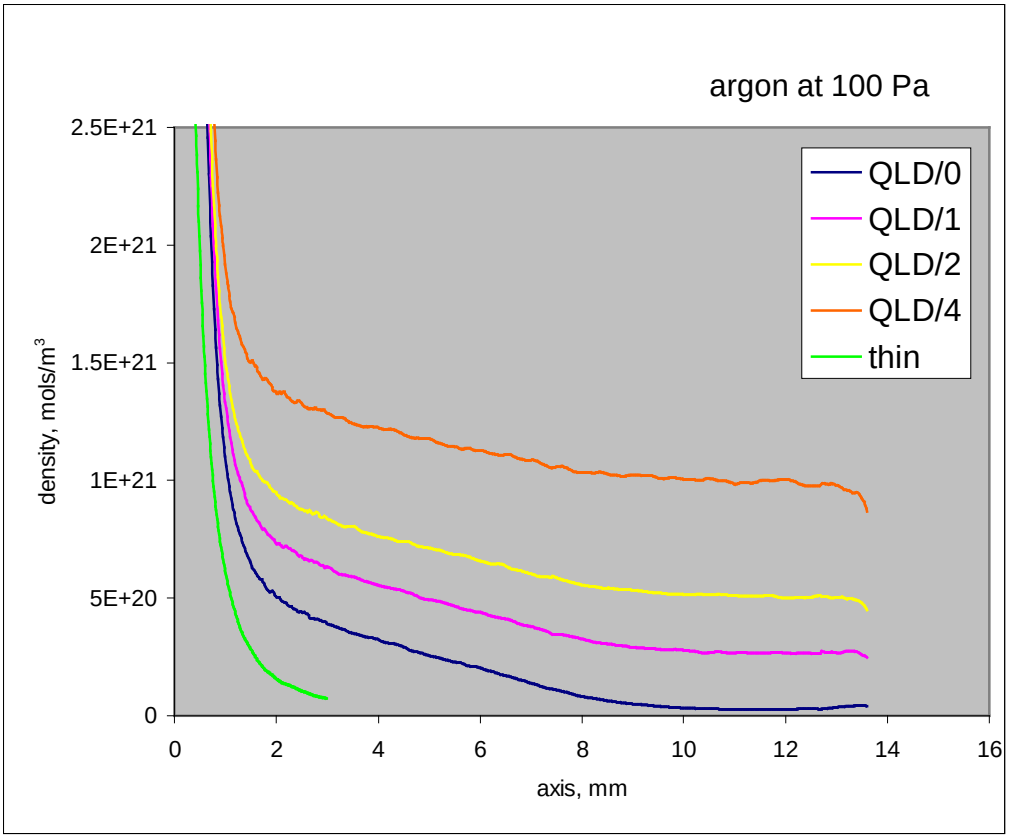

Fig. 6 Density variation of the jet of argon downstream of the PLA plane for the QLD system at four pump pressures, with 100 Pa at the specimen chamber. The "thin" case is reproduced from Fig. 4.

Fig 7 shows the variation of gas density along the axis of the QLD system, when the specimen chamber is held at 1000 Pa and the pump pressure is 0, 10, 20 and 40 Pa. For comparison, the ideal case curve (at 0 Pa pump pressure) is also included.

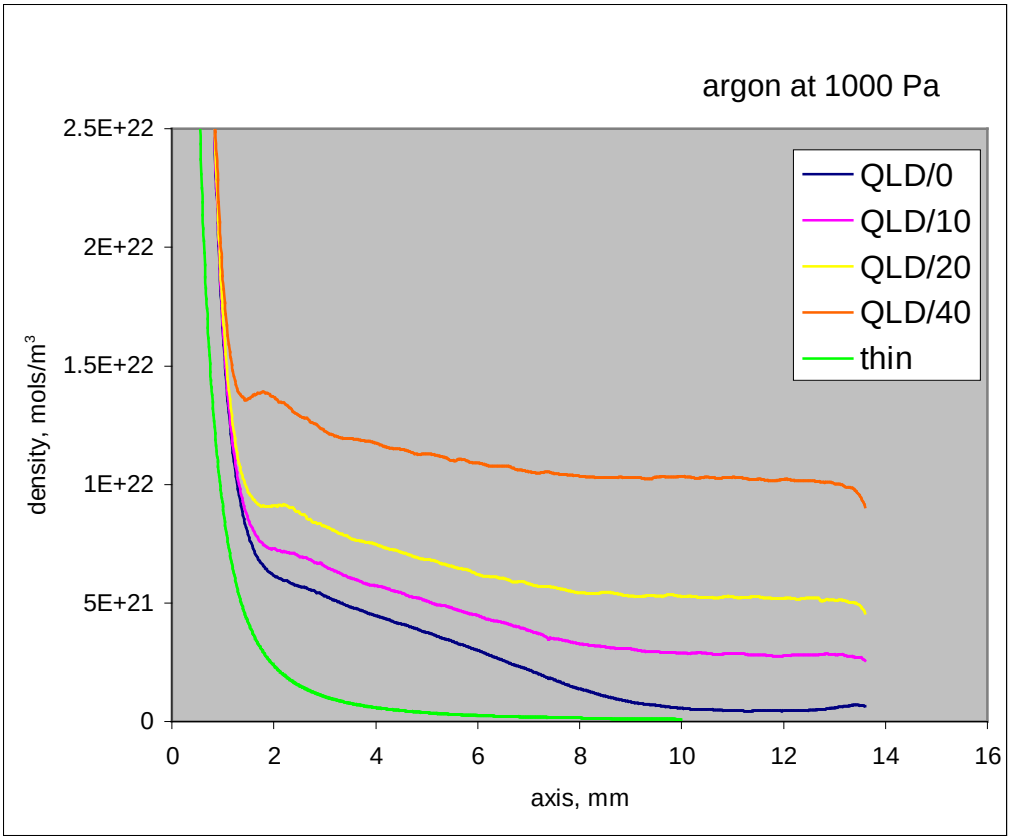

Fig. 7 Density variation of the jet of argon downstream of the PLA plane for the QLD system at four pump pressures, with 1000 Pa at the specimen chamber. The "thin" case is reproduced from Fig. 5.

Fig 8 shows the variation of gas density along the axis of the UTS system, when the specimen chamber is held at 1000 Pa and the pump pressure is 0, 10, 20 and 40 Pa. For comparison, the ideal case curve (at 0 Pa pump pressure) is also included.

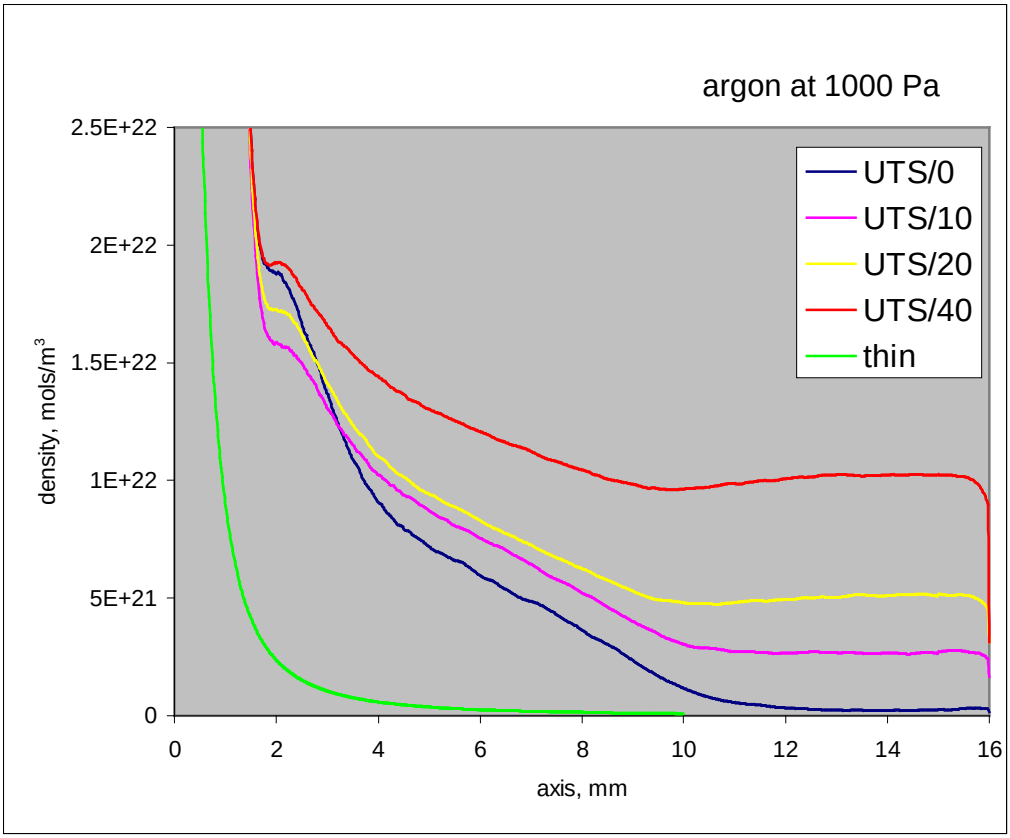

Fig. 8 Density variation of the jet of argon downstream of the PLA plane for the UTS system at four pump pressures, with 1000 Pa at the specimen chamber. The "thin" case is reproduced from Fig. 5.

Finally, a graphical representation of the transmitted electron fraction is shown in Fig. 9 for some typical cases: The fraction is given for all three systems with specimen chamber either at 100 or 1000 Pa but with 0 Pa pump pressure. The QLD and UTS systems are also graphed for 20 Pa pump pressure.

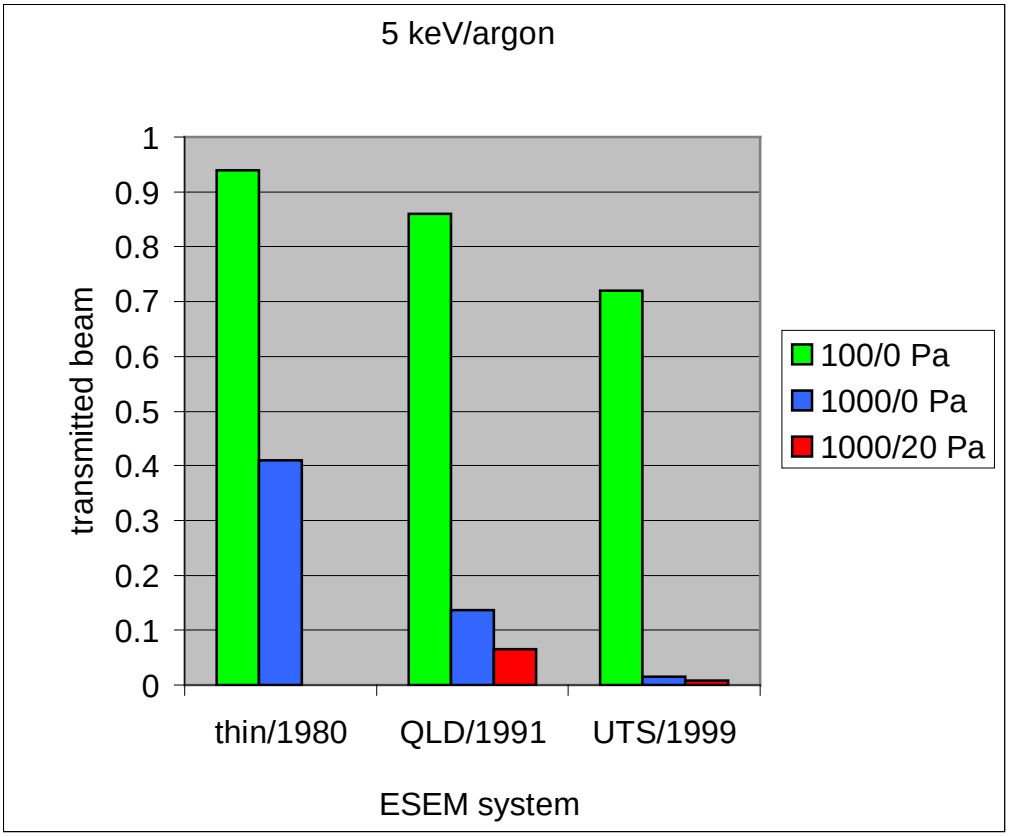

Fig. 9 Transmitted fraction of a 5 keV electron beam through the thin, QLD and UTS systems of PLA .

Discussion

The variation of density and molecular thickness for argon "above" the PLA has been established for an optimum (i.e. "thin") and two commercial ESEM systems. Based on the molecular thickness found, the fraction of electron beam that is totally unaffected in its path through the PLA system has been calculated for four accelerating beam voltages. The electron beam continues to suffer even greater losses as it traverses a gas layer in the specimen chamber before it strikes a specimen, the details of which have been presented previously (Danilatos, 1993). Here, a comparative study of the behavior of different systems, which can be characterized mainly by the gas above the PLA plane has been presented. The effects in the neighborhood immediately below the PLA are generally of a second order. The latter effects can be incorporated in a later complete study involving the positioning of a specimen which yields an optimum imaging condition.

From Table 1, we find that in all cases there is sufficient electron beam probe left for imaging even for an accelerating voltage as low as 5 keV at 100 Pa of argon

in the specimen chamber. An even better situation is expected with gases having lower scattering cross-section such as water vapor and nitrogen, since the present author has reported good imaging at pressures greater than 1000 Pa at 5 keV.

From Table 2, we find that both commercial instruments perform well at 100 Pa specimen chamber pressure but serious problems arise as soon as the pressure is raised to 1000 Pa. In particular, the QLD would have a problem operating at 5 keV at 1000 Pa but it could just cope by increasing the accelerating voltage above 15 or 20 keV, provided that the exit pressure at the pump is maintained very low. If the pump pressure is found to be more than, say, 20 Pa, then a significant component of molecular thickness is added as shown in the Table and in Fig. 7. The area under each curve in the corresponding figures represents the molecular thickness and the deviation from the ideal case is clear.

Similarly, from Table, 3 we find a similar but much more accentuated trend for the UTS instrument. In fact, the electron beam losses are dramatic as soon as we reach the 1000 Pa specimen chamber pressure. The difference from the QLD and the ideal case becomes apparent in Figs 4 and 5, and by comparing Figs. 7 and 8.

A comparative presentation is also shown in Fig. 9 for all three systems at their best possible situation, namely, with 0 Pa pump pressure. In particular, the QLD and UTS systems are also shown with pump pressure at 20 Pa. Operation seems impossible with 5 keV and 1000 Pa, with both instruments.

The actual fraction of electron beam scattered (or transmitted) requires measurement of the actual pump pressure. From the four values of pump pressure computed herewith, the corresponding parameters can be interpolated for a given pump pressure. The latter is expected to lie somewhere in the range of pump pressures presented.

To find the effect of electron beam loss with other gases we need to repeat the present study. However, recalling Avogadro's law, which states that equal numbers of different gas particles occupy the same volume at the same temperature and pressure, we may assume that the molecular thickness for different gases is roughly the same. The latter assumption is not strictly correct, because we are dealing with a dynamic situation of gas flow, whereas Avogadro's law applies to static gases, so that the DSMC computation should be applied for each gas separately. However, the main difference with different gases arises from a variation of their scattering cross-section, so that, to a first approximation, we may get an idea of the electron beam losses by applying different scattering cross-sections to the molecular thickness tabulated herewith.

One remedy to overcome the electron beam loss problem is use very high accelerating voltage, but this is not desirable in most applications. Especially

with organic and insulating specimens, use of high accelerating voltages results in large specimen interaction volumes (or beam penetration) which usually results in specimen damage, instability, and loss of resolution in the backscattered electron mode of detection, in particular.

Another remedy to said problems is to use a smaller diameter PLA which will reduce the over all molecular thickness. However, this also reduces the field of view at low magnifications, which may be undesirable for many applications.

The best solution when using conventional differential pumping system is to redesign the ESEM instrument to allow incorporation of an optimum PLA configuration. Apart from a thin plate PLA, a conical geometry has also been studied by Danilatos (1993). The determination of optimum thickness, cone angle, distance between the two PLAs and the interplay of these parameters will be the subject of further work.

However, it is possible to overcome the natural limit posed by the gas jet if we use the novel method of a reverse flow PLA (RF-PLA) announced recently (Danilatos, 1999). According to the RF-PLA, an annular supersonic gas jet is introduced in the opposite direction around the PLA with a pumping action at its core. By such mechanism, the conventional gas jet “above” the PLA is eliminated. As a result, the electron beam is effectively free to travel and suffers no loss above the PLA.

Another consideration is the study of distribution of electrons lost (or removed) from the electron beam into what has been termed “electron skirt”. This is particularly important in x-ray microanalysis. The study of electron skirt can be done experimentally, theoretically and computationally. All hitherto studies assume an abrupt, or step-wise function of the gas density involved, i.e. the electron beam encounters no gas up to the PLA plane and then it travels through a uniform gas layer in the specimen chamber. However, the present study has shown that the gas has a significant density, which results in a significant electron loss “above” the PLA. In other words, a significant electron skirt has already formed prior to the beam entering the specimen chamber. Any future computation of electron skirt incident on a specimen surface has to account also for the gas density variation both in the depletion zone “below” and in the gas jet “above” the PLA. The DSMC method has provided the density at every point in the entire gas flow field, which can be used as input to any future calculations of electron skirt distributions.

Conclusion

The conventional differential pumping system is characterized by a supersonic gas jet formed downstream of a PLA. The gas jet represents a mass-thickness, which the electron beam of an ESEM must overcome, before it enters in the

specimen chamber. The mass-thickness results in certain amount of electron beam loss. The gas density variation in the jet has been computed by the DSMC method. These computations have been made for a thin plate PLA, which represents a natural limit of mass thickness. Two commercial ESEM instruments have also been studied and found to incur much greater losses. As a consequence, these instruments cannot operate with an accelerating voltage of 5 keV, at 1000 Pa pressure of argon in specimen chamber, while an optimum PLA design normally allows these conditions. Quantitative studies to determine optimum conventional differential pumping systems can be done with the DSMC method.

References

Bird, GA (1985) Molecular Gas Dynamics and the Direct Simulation of Gas Flows, Oxford Science Publications, Clarendon Press, Oxford.

Danilatos GD (1981) Design and construction of an atmospheric or environmental SEM (Part 1). Scanning 4:9-20.

Danilatos GD (1983) Design and construction of an atmospheric or environmental SEM-2. Micron 14:41-52.

Danilatos GD (1988) Foundations of environmental scanning electron microscopy. Advances Electronics Electron Physics 71:109-250.

Danilatos GD (1991) Gas flow properties in the environmental SEM. Microbeam Analysis-1991 (Ed. Howitt DG), San Francisco Press, San Francisco, pp. 201-203.

Danilatos GD (1993) Bibliography of environmental scanning electron microscopy. Microsc. Res. Technique 25:529-534.

Danilatos GD (1993) Environmental scanning electron microscope: Some critical issues. Scanning Microscopy Supplement 7:57-80

Danilatos GD (1999) Reverse flow pressure limiting aperture (RF-PLA). Microscopy and Microanalysis (in press).

Jost K and Kessler J (1963) Die Ortsverteilung mittelschneller Elektronen bei Mehrfachstreung, Zeits. Phys. 176:126-142.